ACS APPLIED MATERIALS & INTERFACES

Research Article

www.acsami.org

Electrochemical Intercalation of Lithium Ions into $NbSe_2$ Nanosheets

Emily Hitz,[†,⊥] Jiayu Wan,[†,⊥] Anand Patel,[‡] Yue Xu,[†] Louisa Meshi,[‡,§] Jiaqi Dai,[†] Yanan Chen,[†] Aijiang Lu,[†] Albert V. Davydov,[*,‡] and Liangbing Hu[*,†]

[†]Department of Materials Science and Engineering, University of Maryland, College Park, Maryland 20742, United States

[‡]Materials Science and Engineering Division, National Institute of Standards and Technology, Gaithersburg, Maryland 20878, United States

[§]Department of Materials Engineering, Ben Gurion University of the Negev, Beer Sheva 84105, Israel

ABSTRACT: Transition metal dichalcogenides (TMDCs) have been known for decades to have unique properties and recently attracted broad attention for their two-dimensional (2D) characteristics. $NbSe_2$ is a metallic TMDC that has been studied for its charge density wave transition behavior and superconductivity but is still largely unexplored for its potential use in engineered devices with applications in areas such as electronics, optics, and batteries. Thus, we successfully demonstrate and present evidence of lithium intercalation in $NbSe_2$ as a technique capable of modifying the material properties of $NbSe_2$ for further study. We demonstrate successful intercalation of Li ions into $NbSe_2$ and confirm this result through X-ray diffraction, noting a unit cell size increase from 12.57 to 13.57 Å in the *c* lattice parameter of the $NbSe_2$ after intercalation. We also fabricate planar half-cell electrochemical devices using ultrathin $NbSe_2$ from platelets to observe evidence of Li-ion intercalation through an increase in the optical transmittance of the material in the visible range. Using 550 nm wavelength light, we observed an increase in optical transmittance of 26% during electrochemical intercalation.

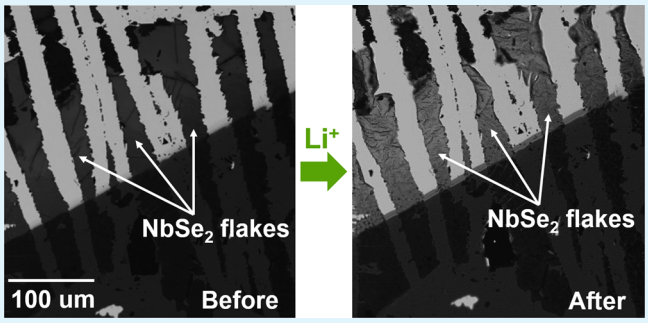

KEYWORDS: *electrochemical intercalation, niobium selenide, 2D materials, lithium, transparent electrodes*

INTRODUCTION

A class of materials known as transition metal dichalcogenides (TMDCs) has been under renewed study due to recent advancements made in the area of layered two-dimensional (2D) materials, particularly with graphitic films for applications in electronics, optoelectronics, and electrochemical devices.[1−5] As layered materials, TMDCs are known to exhibit a wide range of unique mechanical, electrical, and chemical properties that rival the advanced performance standards of other 2D materials such as graphene and BN.[6−15] While TMDCs have been under study for decades, efforts within the scientific and engineering community to study the properties of these unique materials have strengthened again in large part due to recent advances in sample preparation and handling of 2D materials.[16−20]

Many layered materials have been found to participate in a process called intercalation, which allows various molecules to be inserted and stored within a host crystal structure.[21−27] These materials, especially in their 2D morphology, can provide energy storage capabilities[28] while also having the potential to meet concerns that are specific to the modern world, that is, their extraordinary optoelectronic properties[29−31] and mechanical flexibility.[32,33] Intercalation has been used as a technique to further enhance the properties of these materials for their optical, thermal, magnetic, and electronic behavior.[34−41]

TMDCs are materials composed of stacks of atomically thin sheets having the chemical form MX_2, in which M is a transition metal (W, Mo, Nb) and X is a chalcogen (S, Se, Te). For $NbSe_2$, each constituent nanosheet has hexagonal structure in which one atomic layer of niobium is sandwiched between two atomic layers of selenium. Atoms are covalently bonded within the three-atom-thick layers, while van der Waals forces between the layers allow them to remain together. $NbSe_2$ has metallic conductivity at ambient conditions with superconducting and charge density wave transitions at low temperatures.[42−44] Compared to its 2D "cousin" graphene, $NbSe_2$ is still largely unexplored for its chemical and physical properties.[45,46]

In this work, we demonstrate a viable and accessible technique for modifying the properties of 2D $NbSe_2$ to allow for greater depth of study of the material's thermal, chemical, and optical behavior. Our approach relies upon electrochemical intercalation of an alkali metal ion, in this case lithium, into a layered material, which gives rise to specific optical and chemical changes.[47,48] We provide evidence of these changes and characterization of the material system through high-resolution transmission electron microscopy (HRTEM),

Received: November 28, 2015
Accepted: April 21, 2016
Published: April 21, 2016

 © 2016 American Chemical Society

DOI: 10.1021/acsami.5b11583
ACS Appl. Mater. Interfaces 2016, 8, 11390−11395

electrochemical investigations, optical microscopy, and X-ray diffraction (XRD) methods.

RESULTS AND DISCUSSION

For this investigation, we synthesized layered $NbSe_2$ in both powder and platelet form via the chemical vapor transport method. The $NbSe_2$ powder was used as the active material in coin cell electrodes for electrochemical testing (Figure 1a,b),

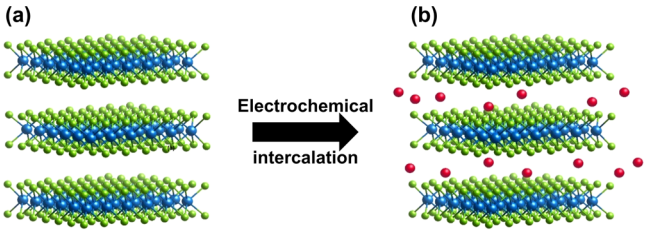

Figure 1. (a) A detailed look at the atomic structure of two-dimensional nanosheets of 2H-$NbSe_2$, each composed of one atomic layer of Nb sandwiched between two layers of Se. (b) Through electrochemical cycling, lithium ions permeate the layered structure of $NbSe_2$, demonstrating its charge storage capability.

while single-crystal $NbSe_2$ platelets were used to fabricate planar devices for observation of the optical behavior of the material. A detailed enumeration of relevant techniques can be found in the Experimental Procedures section.

It is well-documented in previous research efforts on 2D materials that the electrochemical processes associated with lithium intercalation in TMDCs are often complex, involving both reversible and nonreversible reactions and having multiple lithiation/delithiation stages. With the likelihood of a complex system taken into consideration, our goal was to study the structural and compositional behavior of the electrochemical lithiation process in $NbSe_2$. We first performed cycling and cyclic voltammetry (CV) electrochemical studies on coin cells (half cell with Li as counter electrode) containing an $NbSe_2$-based cathode in the voltage range of 0−3 V, which was found to have many stages of lithiation reactions present. We exclude this regime from our focus of discussion. After further electrochemical studies, it was found that cycling the coin cells within the voltage range of 1−3 V allowed the system to stay within a simpler lithiation/delithiation regime. To characterize the system of lithium intercalation in $NbSe_2$, we present data on the electrochemical behavior of coin cells cycled between 1 and 3 V with a current density of 50 mA/g. An electrochemical workstation (Biologic SP-150)[49] was used to acquire the charge−discharge voltage profile of the coin cells. The cells showed reasonably high specific capacity, as shown in the charge−discharge curves for the first three cycles (Figure 2a). The charge capacity of the cell was observed to be 372 mAh/g for the first cycle. On the second and third charge cycles, we observed a specific capacity of 342 mAh/g and 336 mAh/g, respectively. The discharge capacity of the cell exhibited a larger decrease in the capacitance after the first cycle than was observed correspondingly when charging the cell. During the first discharge cycle, a specific capacity of 534 mAh/g was observed. On the second and third discharge cycles, the specific capacity decreased to 347 mAh/g and 332 mAh/g, respectively. According to the reversible specific capacity of Li-$NbSe_2$ cycled from 1−3 V, the number of Li ions intercalated per $NbSe_2$ is calculated to be 3.48, corresponding to the formation of $Li_{3.48}NbSe_2$. Results give evidence of at least one nonreversible reaction occurring in the system at 1.22 V, which can also be seen in Figure 2, panel b in the CV curve for cycle 1. The cells otherwise demonstrate good reversibility after the first cycle. In Figure 2, panel b, CV curves for the first three cycles are shown, which confirm the voltage levels at which of the reactions present within the system occur. Reversible reactions are observed at 1.55 V, 1.99 V (cathodic), and 2.74 V (anodic).

While electrochemical studies allowed us to characterize the evolution of lithium intercalation in $NbSe_2$, indexing of XRD peaks for discharged coin cell cathodes was crucial in our investigation of the structure and identity of the lithiated material. The results of this analysis can be seen in Figure 3, panels a and b. We first characterized the Li-intercalated-$NbSe_2$ system by performing XRD on the as-prepared $NbSe_2$-based coin cell electrodes to verify the composition and structure of the material. A peak identification analysis was performed on the spectra of the $NbSe_2$-based cathode prior to electrochemical discharge. Upon comparison with literature sources for peak information,[50,51] presence of hexagonal phase 2H-$NbSe_2$ was detected. The material is known to be of the $P6_3mmc$ (194) space group, with the following lattice parameters: a = 3.44 Å and c = 12.55 Å. Experimentally, the lattice spacing of our material agreed well with the literature; through profile

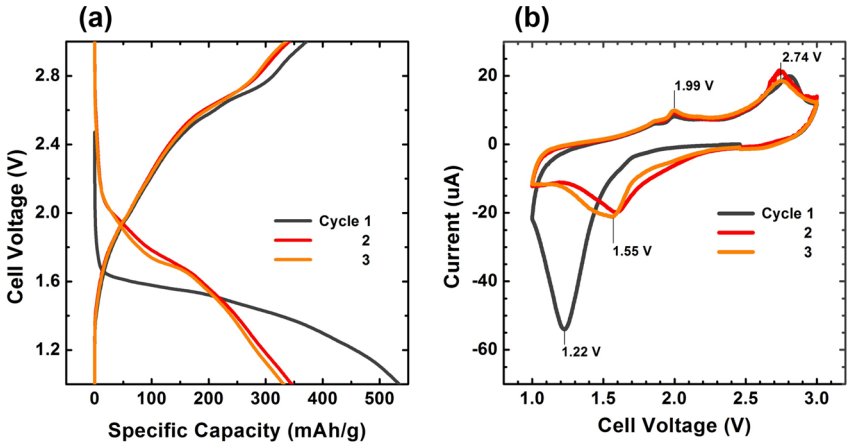

Figure 2. Studies of electrochemical intercalation of Li ion in $NbSe_2$-based electrodes. (a) Cycling behavior of the $NbSe_2$-based cathode. (b) CV curves of the first three cycles of the $NbSe_2$-based cathode. A voltage range of 1−3 V is selected to prevent solid−electrolyte interface formation.

DOI: 10.1021/acsami.5b11583
ACS Appl. Mater. Interfaces 2016, 8, 11390−11395

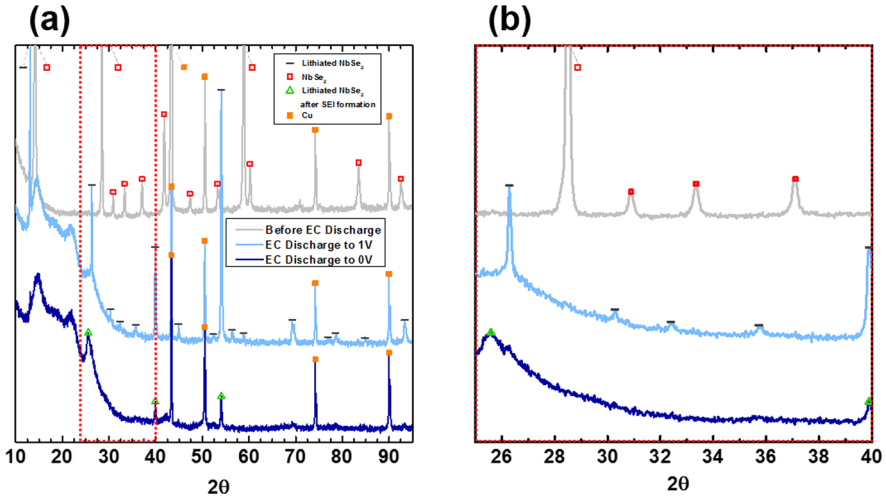

Figure 3. (a) Full and (b) zoomed-in from 25° to 40°, XRD patterns of the $NbSe_2$-based cathode with carbon black additive and PVP polymer binder before and after electrochemical intercalation. After electrochemical discharge to 1 V, the presence of lithium via a change in the crystal unit cell size is evident, and after electrochemical discharge to 0 V, presence of Li and irreversible formation of a solid electrolyte interface layer is demonstrated.

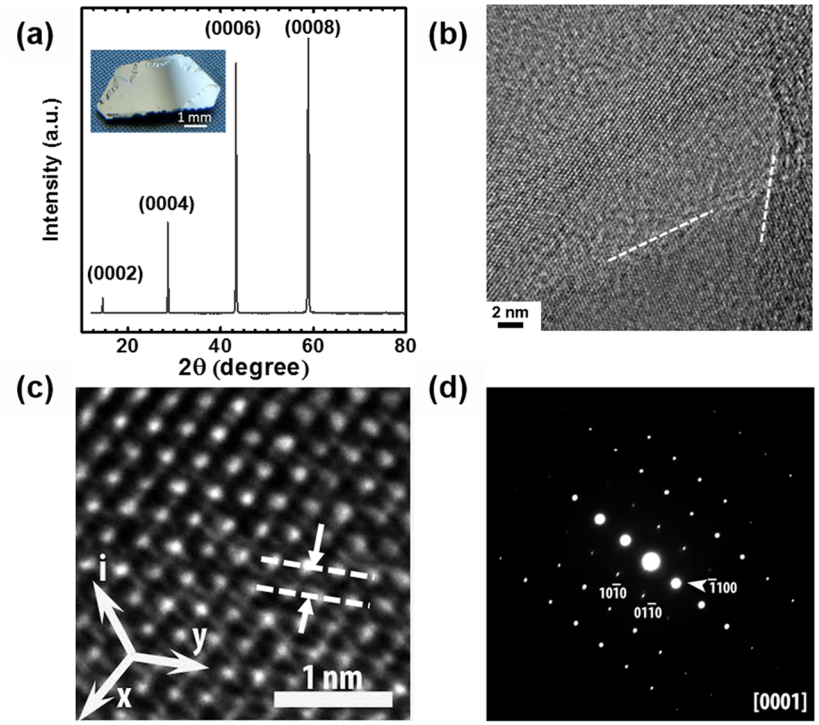

Figure 4. (a) XRD from $NbSe_2$ platelets, (b) HRTEM image of $NbSe_2$ platelets sample, and (c) magnified HRTEM image of the same $NbSe_2$ platelet with crystallographic axes denoted; (d) electron diffraction taken at [0001] orientation of the $NbSe_2$ flake.

matching using a Le Bail fit with (TOPAS analysis software), the $NbSe_2$-based cathode sample was identified to have an *a* parameter of 3.4437(3) Å and a *c* parameter of 12.5668(3) Å. Elemental Cu in its cubic form was also detected. The presence of Cu in the X-ray diffractogram can be attributed to the copper foil current collector on which the slurry was deposited.

After electrochemical discharge from the intrinsic open circuit voltage of the cell to 1 V, we observed a preservation of the layered $NbSe_2$ structure, as indicated by the results of the peak identification. Because of the air-sensitivity of the discharged cathodes, Kapton tape was placed over the samples, which resulted in an observation of background diffraction from 10° to 30°. Profile matching using a Le Bail fit was performed on the XRD pattern for the cell discharged to 1 V. The results of this analysis showed that the unit cell size of the crystal increased upon discharge to 1 V, as a left-shift of the $NbSe_2$ peaks occurred. Most notably, the *c* parameter increased from 12.5668(3) Å before intercalation to 13.5702(5) Å, while the *a* parameter remained approximately unchanged at 3.4311(2) Å. An increase in the unit cell size in the direction of the *c* parameter corresponds to an increase in the interlayer spacing. We attribute this change in the interlayer spacing to the presence of lithium ions after intercalation.

DOI: 10.1021/acsami.5b11583
ACS Appl. Mater. Interfaces 2016, 8, 11390−11395

As shown in Figure 3, panels a and b, electrochemical discharge of a cell to 0 V resulted in a very different crystal structure than the discharge to 1 V. After peak identification, we observed a decreased relative intensity of $NbSe_2$ peaks to Cu peaks and an even larger left shift of $NbSe_2$ peaks for the region of 25° to 40° (Figure 3b). We attribute the left shift again to an increase in the *c*-axis to 13.57 Å due to Li intercalation in between the $NbSe_2$ layers and the lower relative intensity to the destruction of material during large amounts of lithiation.

In the previous section, we used $NbSe_2$ powder as active material to show that Li ion can electrochemically intercalate in the material. To further demonstrate Li-ion intercalation in 2D $NbSe_2$ materials and the optical and structural changes that occur, we prepared $NbSe_2$ by the chemical vapor transport method. Figure 4, panel a inset shows the truncated trapezoid-shaped platelet with a [000l] basal facet is about 200 nm thick. The XRD peaks of the $NbSe_2$ platelet are at 14.46°, 28.56°, 43.32°, and 58.89°, which correspond to the (0002), (0004), (0006), and (0008) lattice planes of the 2H $NbSe_2$ ($P6_3/mmc$ (194); PDF#87−24015), with *c* lattice parameter of 12.570 Å. This XRD result clearly shows the $NbSe_2$ platelet we prepared is single crystalline. Transmission electron microscopy (TEM) was also utilized to characterize the $NbSe_2$ platelet. The stoichiometry was verified using standardless X-ray energy dispersive spectroscopy (EDS) in TEM. Figure 4, panel b shows the HRTEM image of the single crystalline $NbSe_2$. The dashed lines in the image indicate edges of areas with different thickness, which illustrate the layered nature of the material. Figure 4, panel c shows a magnified HRTEM image of the same sample. An interplanar distance of $d_{10.0}$ = 2.98 ± 0.04 Å is marked on the image. The selected area electron diffraction (SAED) pattern of $NbSe_2$ taken along [0001] direction is shown in Figure 4, panel d.

Planar batteries were built to study the optical properties of the $NbSe_2$ upon lithiation. As shown in a schematic image of the $NbSe_2$ planar battery in Figure 5, panel a, a thin flake of $NbSe_2$ and a small pellet of Li metal serve as working and counter electrodes on a glass cover slide, while Cu current collectors are applied via thermal evaporation on the substrate. The $NbSe_2$ platelet is mechanically exfoliated and deposited on a clean glass cover slide prior to Cu deposition. Figure 5, panels b and c show the optical image of the $NbSe_2$ thin films by optical microscopy before and after Li intercalation at 550 nm wavelength light. The $NbSe_2$ flakes initially appear very dark in the micrograph, with an optical transmittance of 25%. After intercalation, the lithiated $NbSe_2$ flake shows a much lighter color in the image, with an optical transmittance of 51%. We also observed a wrinkle formation in the $NbSe_2$ thin film after lithiation, which arises from the volume expansion of the electrode material after Li-ion intercalation, typically seen in in battery electrodes.[34,52−54] Figure 5, panel d shows the optical transmittance of the $NbSe_2$ thin film before and after intercalation at wavelengths of 450 nm, 550 nm, and 750 nm, in which the transmittance increased from 24.3% to 49.7%, 27.5% to 54.5%, and 56.4% to 66.5%, respectively. Upon further analysis and computer simulation of intercalation, it was found that as the concentration of Li increased, the lattice paramater vertical to the layer surface increased remarkably. As a consequence, the overlap of the electron clouds between the layers decreased, and the band structure changed accordingly. The width of the energy bands decreased so that the interband transitions must take place at higher energies. With this, we saw a blue-shift in the overall dielectric function of the material, which corresponds to a dramatic change in transmittance. The two-fold transmittance increase as well as wrinkle formation confirm the successful intercalation of Li ion in the $NbSe_2$ thin film.

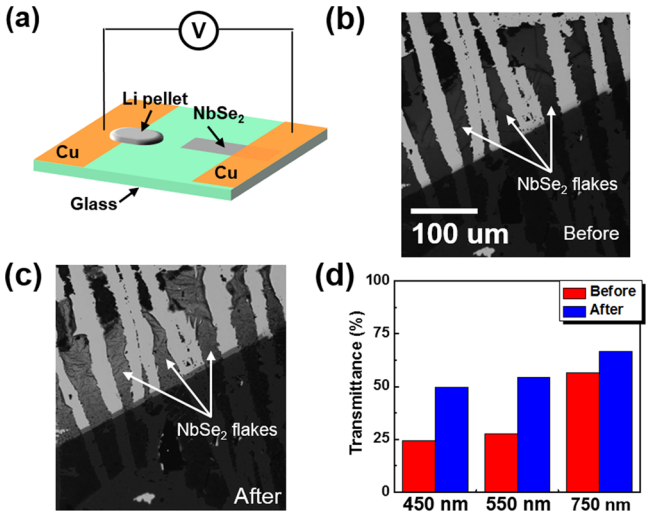

Figure 5. (a) Schematic of lithium intercalation in $NbSe_2$ with microbattery. (b) $NbSe_2$ flakes before electrochemical intercalation of lithium and (c) after lithium intercalation and electrochemical discharge to 0 V, both images taken under a wavelength of 550 nm. (d) Comparison of transmittance change observed for lithium intercalation at different wavelengths of light.

■ CONCLUSIONS

Through electrochemical and XRD studies, we provide evidence of lithium intercalation in 2H-$NbSe_2$ via an electrochemical method. In the electrochemical studies, we observed reversible and irreversible changes within a cycling voltage range of both 1−3 and 0−3 V. We confirm that the electrochemical lithiation mechanism in $NbSe_2$ proceeds with Li intercalation between the $NbSe_2$ layers rather than a conversion reaction commonly observed in other TMDCs (i.e., MoS_2) by XRD analysis. Though it can be readily calculated from the XRD pattern directly, we performed structure refinement to reveal an increase in the interplanar spacing by approximately 1 Å, which we claim is due to the presence of Li ion. From the cycling results, we confirmed that 3.48 Li ions are reversibly intercalated for every $NbSe_2$ formula unit when discharged to 1 V. We support this claim with a corresponding result in the optical observation of electrochemical devices fabricated with thin flakes derived from $NbSe_2$ in the platelet form. From in situ measurements of the change in flake transmittance during electrochemical discharge, we observed an increase in the transmittance. This result confirms successful intercalation of Li ions into $NbSe_2$.

■ EXPERIMENTAL PROCEDURES

$NbSe_2$ Powder Synthesis. Stoichiometric amounts of Nb and Se elemental powders were sealed in a quartz ampule under vacuum and annealed in a tube furnace at 850 °C for 84 h followed by cooling at 5 °C/min rate down to 400 °C and then being removed from the furnace. The reaction product was confirmed by XRD analysis to be pure polycrystalline $NbSe_2$.

$NbSe_2$ Platelet Growth. The $NbSe_2$ platelets were synthesized using the chemical vapor transport (CVT) method. A sample of

DOI: 10.1021/acsami.5b11583
ACS Appl. Mater. Interfaces 2016, 8, 11390−11395

0.9906 g of $NbSe_2$ polycrystalline powder was compressed into a pellet and sealed under vacuum in a quartz ampule with 66.5 mg of iodine added (equivalent to 4 mg/cm^3 of I_2 concentration in the ampule), where iodine served as a transport agent in the CVT process. The ampule was heat treated in a horizontal tube furnace at 825 °C for 84 h, which resulted in the growth of single-crystalline platelets of $NbSe_2$, confirmed by XRD and TEM.

2D-Planar Device Fabrication. For the 2D planar devices, we used the single crystalline platelet form of $NbSe_2$. After preparing a glass cover slide by sonication in acetone and then methanol, we mounted it to a glass slide with Scotch tape. Via mechanical exfoliation, we prepared the sample on the glass slide and observed thin flakes of $NbSe_2$ under an optical microscope. The full device was then assembled by depositing copper current collectors that would form electrical connections between the flake and the rest of the device. The device was then finished by constructing a small chamber in which the $LiPF_6$ in EC/DEC (w/w = 1:1) electrolyte could be contained, filling the chamber in argon atmosphere, and sealing the device with another slide cover using epoxy glue.

Coin Cell Device Fabrication. Coin cells were fabricated using $NbSe_2$ powder as the active material of the cathode. A slurry mixture was first prepared with $NbSe_2$ as the main component by adding acetylene black carbon as a conductive additive consistent with other electrochemical cell preparation techniques, and polyvinylpyrrolidone (PVP) as a binding agent. The slurry was combined in proportions of 7:2:1 $NbSe_2$/acetylene black/PVP by using water as the solvent. Once all components were evenly combined using a mortar and pestle, the mixture was deposited on clean copper foil using the doctor blade coating method and transferred to a vacuum oven at approximately 100 °C to allow the coating to dry completely. After, punches were used to prepare PVP separator and electrodes for coin cell assembly. In argon atmosphere, Li metal (Sigma-Aldrich), two sheets of PVP separator, lithium hexafluorophosphate solution in ethylene carbonate and diethyl carbonate (1 M $LiPF_6$ in EC/DEC w/w = 1:1) electrolyte, and the $NbSe_2$-based electrode were arranged in 20 mm diameter 304 stainless steel coin cell cases. The assembly was then crimped at approximately 1000 psi to form a functional coin cell device.

Preparation of $NbSe_2$ Cathodes for XRD Analysis. To perform XRD on the intercalated $NbSe_2$ coin cell devices, it was first necessary to remove the $NbSe_2$-containing electrodes from the coin cells. This task was made more challenging due to the sensitivity of the compounds to the atmosphere. We mitigated this concern by disassembling the coin cells inside a glovebox with argon atmosphere. The samples were mounted for XRD analysis while still inside the glovebox by applying Kapton polyimide film with silicone adhesive overtop each electrode. We intentionally prevented the tape from coming into contact with the sample directly, thus preventing contamination of the sample while still allowing an inert environment to be maintained during XRD analysis. XRD analysis was carried out on a D8 Advance with LynxEye and SolX capabilities.

Preparation of the $NbSe_2$ Flakes for TEM Analysis. For TEM investigation, the $NbSe_2$ flake was mounted using epoxy on a Cu TEM grid with an oval hole. Then, by using the "Scotch tape" method, the flake layers were removed to reduce the thickness to minimum (about 15 μm). Final thinning was performed by Ar ions in a precision ion polishing system (PIPS, Gatan). TEM, EDS, and HRTEM studies were carried out on 300 kV Titan, FEI electron microscope.

AUTHOR INFORMATION

Corresponding Authors

*E-mail: binghu@umd.edu.

*E-mail: albert.davydov@nist.gov.

Author Contributions

⊥These authors contributed equally to this work.

Notes

The authors declare no competing financial interest.

ACKNOWLEDGMENTS

This work was supported by NSF-CBET Award No. 1335979 and internal funding from the National Institute of Standards and Technology Material Measurement Laboratory. The authors thank Irina Kalish from NIST and Christopher Borg from UMD for help with the XRD data analysis.

REFERENCES

(1) Ding, Y.; Wang, Y.; Ni, J.; Shi, L.; Shi, S.; Tang, W. First principles study of structural, vibrational and electronic properties of graphene-like MX_2 (M=Mo, Nb, W, Ta; X=S, Se, Te) monolayers. *Phys. B* **2011**, *406*, 2254−2260.

(2) Schwierz, F. Graphene transistors. *Nat. Nanotechnol.* **2010**, *5*, 487−496.

(3) Avouris, P. Graphene: Electronic and Photonic Properties and Devices. *Nano Lett.* **2010**, *10*, 4285−4294.

(4) Lee, J.; Lee, S.; Paik, U.; Choi, Y. Aqueous processing of natural graphite particulates for lithium-ion battery anodes and their electrochemical performance. *J. Power Sources* **2005**, *147*, 249−255.

(5) Bang, G. S.; Nam, K. W.; Kim, J. Y.; Shin, J.; Choi, J. W.; Choi, S. Effective Liquid-Phase Exfoliation and Sodium Ion Battery Application of MoS_2 Nanosheets. *ACS Appl. Mater. Interfaces* **2014**, *6*, 7084−7089.

(6) Bunch, J. S.; Verbridge, S. S.; Alden, J. S.; van der Zande, A. M.; Parpia, J. M.; Craighead, H. G.; McEuen, P. L. Impermeable Atomic Membranes from Graphene Sheets. *Nano Lett.* **2008**, *8*, 2458−2462.

(7) Lee, C.; Wei, X.; Kysar, J. W.; Hone, J. Measurement of the Elastic Properties and Intrinsic Strength of Monolayer Graphene. *Science* **2008**, *321*, 385−388.

(8) Subrahmanyam, K. S.; Kumar, P.; Maitra, U.; Govindaraj, A.; Hembram, K. P. S. S.; Waghmare, U. V.; Rao, C. N. R. Chemical storage of hydrogen in few-layer graphene. *Proc. Natl. Acad. Sci. U. S. A.* **2011**, *108*, 2674−2677.

(9) Stephenson, T.; Li, Z.; Olsen, B.; Mitlin, D. Lithium ion battery applications of molybdenum disulfide (MoS2) nanocomposites. *Energy Environ. Sci.* **2014**, *7*, 209−231.

(10) Ayari, A.; Cobas, E.; Ogundadegbe, O.; Fuhrer, M. S. Realization and electrical characterization of ultrathin crystals of layered transition-metal dichalcogenides. *J. Appl. Phys.* **2007**, *101*, 014507.

(11) Balandin, A. A.; Ghosh, S.; Bao, W.; Calizo, I.; Teweldebrhan, D.; Miao, F.; Lau, C. N. Superior Thermal Conductivity of Single-Layer Graphene. *Nano Lett.* **2008**, *8*, 902−907.

(12) Mak, K. F.; He, K.; Shan, J.; Heinz, T. F. Control of valley polarization in monolayer MoS2 by optical helicity. *Nat. Nanotechnol.* **2012**, *7*, 494−498.

(13) Wang, Q. H.; Kalantar-Zadeh, K.; Kis, A.; Coleman, J. N.; Strano, M. S. Electronics and optoelectronics of two-dimensional transition metal dichalcogenides. *Nat. Nanotechnol.* **2012**, *7*, 699−712.

(14) Tsai, D.; Liu, K.; Lien, D.; Tsai, M.; Kang, C.; Lin, C.; Li, L.; He, J. Few-Layer MoS_2 with High Broadband Photogain and Fast Optical Switching for Use in Harsh Environments. *ACS Nano* **2013**, *7*, 3905−3911.

(15) Ozdemir, B.; Barone, V. Structural and electronic properties of crystalline graphite-like BC3. *Comput. Mater. Sci.* **2015**, *109*, 248−252.

(16) O'Neill, A.; Khan, U.; Coleman, J. N. Preparation of High Concentration Dispersions of Exfoliated MoS_2 with Increased Flake Size. *Chem. Mater.* **2012**, *24*, 2414−2421.

(17) Novoselov, K. S.; Jiang, D.; Schedin, F.; Booth, T. J.; Khotkevich, V. V.; Morozov, S. V.; Geim, A. K. Two-dimensional atomic crystals. *Proc. Natl. Acad. Sci. U. S. A.* **2005**, *102*, 10451−10453.

(18) Zeng, H.; Zhi, C.; Zhang, Z.; Wei, X.; Wang, X.; Guo, W.; Bando, Y.; Golberg, D. White Graphenes": Boron Nitride Nanoribbons via Boron Nitride Nanotube Unwrapping. *Nano Lett.* **2010**, *10*, 5049−5055.

(19) Zhang, X.; Zhang, D.; Tang, H.; Ji, X.; Zhang, Y.; Tang, G.; Li, C. Facile synthesis and characterization of hexagonal $NbSe_2$ nanoplates. *Mater. Res. Bull.* **2014**, *53*, 96−101.

(20) Bonaccorso, F.; Colombo, L.; Yu, G.; Stoller, M.; Tozzini, V.; Ferrari, A. C.; Ruoff, R. S.; Pellegrini, V. Graphene, related two-

DOI: 10.1021/acsami.5b11583
ACS Appl. Mater. Interfaces 2016, 8, 11390−11395

dimensional crystals, and hybrid systems for energy conversion and storage. *Science* **2015**, *347*, 1246501.
(21) Kumagai, N.; Tanno, K.; Nakajima, T.; Watanabe, N. Electrode reaction of niobium chalcogenides as positive electrodes for secondary lithium batteries. *J. Electroanal. Chem. Interfacial Electrochem.* **1985**, *184*, 87−96.
(22) Wang, Y.; Ou, J. Z.; Balendhran, S.; Chrimes, A. F.; Mortazavi, M.; Yao, D. D.; Field, M. R.; Latham, K.; Bansal, V.; Friend, J. R.; Zhuiykov, S.; Medhekar, N. V.; Strano, M. S.; Kalantar-zadeh, K. Electrochemical Control of Photoluminescence in Two-Dimensional MoS_2 Nanoflakes. *ACS Nano* **2013**, *7*, 10083−10093.
(23) Wang, H.; Yuan, H.; Sae Hong, S.; Li, Y.; Cui, Y. Physical and chemical tuning of two-dimensional transition metal dichalcogenides. *Chem. Soc. Rev.* **2015**, *44*, 2664−2680.
(24) Dresselhaus, M. S.; Dresselhaus, G. Intercalation compounds of graphite. *Adv. Phys.* **2002**, *51*, 1−186.
(25) Chen, K. P.; Chung, F. R.; Wang, M.; Koski, K. J. Dual Element Intercalation into 2D Layered Bi_2Se_3 Nanoribbons. *J. Am. Chem. Soc.* **2015**, *137*, 5431−5437.
(26) Yang, H.; Song, T.; Lee, S.; Han, H.; Xia, F.; Devadoss, A.; Sigmund, W.; Paik, U. Tin indium oxide/graphene nanosheet nanocomposite as an anode material for lithium ion batteries with enhanced lithium storage capacity and rate capability. *Electrochim. Acta* **2013**, *91*, 275−281.
(27) Friend, R. H.; Yoffe, A. D. The lithium intercalates of the transition metal dichalcogenides. *Adv. Phys.* **1987**, *36*, 1.
(28) Uthaisar, C.; Barone, V.; Fahlman, B. D. On the chemical nature of thermally reduced graphene oxide and its electrochemical Li intake capacity. *Carbon* **2013**, *61*, 558−567.
(29) Khrapach, I.; Withers, F.; Bointon, T. H.; Polyushkin, D. K.; Barnes, W. L.; Russo, S.; Craciun, M. F. Novel Highly Conductive and Transparent Graphene-Based Conductors. *Adv. Mater.* **2012**, *24*, 2844−2849.
(30) Wan, J.; Gu, F.; Bao, W.; Dai, J.; Shen, F.; Luo, W.; Han, X.; Urban, D.; Hu, L. Sodium-Ion Intercalated Transparent Conductors with Printed Reduced Graphene Oxide Networks. *Nano Lett.* **2015**, *15*, 3763−3769.
(31) Su, S.; Hsu, Y.; Chang, Y.; Chiu, M.; Hsu, C.; Hsu, W.; Chang, W.; He, J.; Li, L. Band Gap-Tunable Molybdenum Sulfide Selenide Monolayer Alloy. *Small* **2014**, *10*, 2589−2594.
(32) Bae, S.; Kim, H.; Lee, Y.; Xu, X.; Park, J.-S.; Zheng, Y.; Balakrishnan, J.; Lei, T.; Ri Kim, H.; Song, Y. I.; Kim, Y.-J.; Kim, K. S.; Özyilmaz, B.; Ahn, J.-H.; Hong, B. H.; Iijima, S. Roll-to-roll production of 30-in. graphene films for transparent electrodes. *Nat. Nanotechnol.* **2010**, *5*, 574−578.
(33) Xiong, P.; Peng, L.; Chen, D.; Zhao, Y.; Wang, X.; Yu, G. Two-dimensional nanosheets based Li-ion full batteries with high rate capability and flexibility. *Nano Energy* **2015**, *12*, 816−823.
(34) Bao, W.; Wan, J.; Han, X.; Cai, X.; Zhu, H.; Kim, D.; Ma, D.; Xu, Y.; Munday, J. N.; Drew, H. D.; Fuhrer, M. S.; Hu, L. Approaching the limits of transparency and conductivity in graphitic materials through lithium intercalation. *Nat. Commun.* **2014**, *5*, 4224.
(35) Wan, J.; Bao, W.; Liu, Y.; Dai, J.; Shen, F.; Zhou, L.; Cai, X.; Urban, D.; Li, Y.; Jungjohann, K.; Fuhrer, M. S.; Hu, L. In Situ Investigations of Li-MoS_2 with Planar Batteries. *Adv. Energy Mater.* **2015**, *5*.10.1002/aenm.201401742
(36) Kim, N.; Kim, K. S.; Jung, N.; Brus, L.; Kim, P. Synthesis and Electrical Characterization of Magnetic Bilayer Graphene Intercalate. *Nano Lett.* **2011**, *11*, 860−865.
(37) Lu, N.; Guo, H.; Wang, L.; Wu, X.; Zeng, X. C. van der Waals trilayers and superlattices: modification of electronic structures of MoS_2 by intercalation. *Nanoscale* **2014**, *6*, 4566−4571.
(38) Yu, Y.; Yang, F.; Lu, X. F.; Yan, Y. J.; Cho, Y.-H.; Ma, L.; Niu, X.; Kim, S.; Son, Y.; Feng, D.; Li, S.; Cheong, S.; Chen, X. H.; Zhang, Y. Gate-tunable phase transitions in thin flakes of 1T-TaS_2. *Nat. Nanotechnol.* **2015**, *10*, 270−276.
(39) Wu, H.; Kong, D.; Ruan, Z.; Hsu, P.; Wang, S.; Yu, Z.; Carney, T. J.; Hu, L.; Fan, S.; Cui, Y. A transparent electrode based on a metal nanotrough network. *Nat. Nanotechnol.* **2013**, *8*, 421−425.
(40) Li, H.; Pan, W.; Zhang, W.; Huang, S.; Wu, H. TiN Nanofibers: A New Material with High Conductivity and Transmittance for Transparent Conductive Electrodes. *Adv. Funct. Mater.* **2013**, *23*, 209−214.
(41) Acrivos, J.; Liang, W.; Wilson, J. A.; Yoffe, A. D. Optical studies of metal-semiconductor transmutations produced by intercalation. *J. Phys. C: Solid State Phys.* **1971**, *4*, L18.
(42) Mattheiss, L. F. Band Structures of Transition-Metal-Dichalcogenide Layer Compounds. *Phys. Rev. B* **1973**, *8*, 3719−3740.
(43) Wilson, J. A.; Di Salvo, F. J.; Mahajan, S. Charge-density waves and superlattices in the metallic layered transition metal dichalcogenides. *Adv. Phys.* **2001**, *50*, 1171−1248.
(44) Castro Neto, A. H. Charge Density Wave, Superconductivity, and Anomalous Metallic Behavior in 2D Transition Metal Dichalcogenides. *Phys. Rev. Lett.* **2001**, *86*, 4382−4385.
(45) Folinsbee, J. T.; Simpson, A. M.; Jericho, M. H. Li diffusion in $NbSe_2$ and $Ag_{0.25}NbSe_2$ single crystals. *Mater. Res. Bull.* **1986**, *21* (8), 961−969.
(46) Doran, N. J. Electronic Structure and Band Theory of Transition Metal Dichalcogenides. *Physica B+C* **1980**, *99*, 227−237.
(47) Cheng, Y.; Nie, A.; Zhang, Q.; Gan, L.; Shahbazian-Yassar, R.; Schwingenschlogl, U. Origin of the Phase Transition in Lithiated Molybdenum Disulfide. *ACS Nano* **2014**, *8*, 11447−11453.
(48) Nie, A.; Cheng, Y.; Zhu, Y.; Asayesh-Ardakani, H.; Tao, R.; Mashayek, F.; Han, Y.; Schwingenschlögl, U.; Klie, R. F.; Vaddiraju, S.; Shahbazian-Yassar, R. Lithiation-Induced Shuffling of Atomic Stacks. *Nano Lett.* **2014**, *14*, 5301−5307.
(49) Certain commercial equipment, instruments, or materials are identified in this paper to specify the experimental procedure adequately. Such identification is not intended to imply recommendation or endorsement by the National Institute of Standards and Technology nor is it intended to imply that the materials or equipment identified are necessarily the best available for the purpose.
(50) Meerschaut, A.; Deudon, C. Crystal structure studies of the 3R-$Nb_{1.09}S_2$ and the 2H-$NbSe_2$ compounds: correlation between non-stoichiometry and stacking type (= polytypism). *Mater. Res. Bull.* **2001**, *36*, 1721−1727.
(51) Otte, H. M. Lattice Parameter Determinations with an X-Ray Spectrogoniometer by the Debye-Scherrer Method and the Effect of Specimen Condition. *J. Appl. Phys.* **1961**, *32*, 1536−1546.
(52) Cui, L.; Hu, L.; Choi, J. W.; Cui, Y. Light-Weight Free-Standing Carbon Nanotube-Silicon Films for Anodes of Lithium Ion Batteries. *ACS Nano* **2010**, *4*, 3671−3678.
(53) Bao, W.; Miao, F.; Chen, Z.; Zhang, H.; Jang, W.; Dames, C.; Lau, C. N. Controlled ripple texturing of suspended graphene and ultrathin graphite membranes. *Nat. Nanotechnol.* **2009**, *4*, 562−566.
(54) Lacey, S. D.; Wan, J.; Cresce, A. v. W.; Russell, S. M.; Dai, J.; Bao, W.; Xu, K.; Hu, L. Atomic Force Microscopy Studies on Molybdenum Disulfide Flakes as Sodium-Ion Anodes. *Nano Lett.* **2015**, *15*, 1018−1024.

DOI: 10.1021/acsami.5b11583
ACS Appl. Mater. Interfaces 2016, 8, 11390−11395